



Chromite chemistry as petrogenetic indicator of altered ultramafic rocks from Higher Himalayan Crystalline, Kishtwar, India

PAWAN SINGH^{1,*} and PANKAJ KUMAR SRIVASTAVA²

¹Geological Survey of India, SU: Madhya Pradesh, Bhopal 462 016, India.

²Department of Geology, University of Jammu, Jammu 180 006, India.

*Corresponding author. e-mail: psp.geo.ju@gmail.com

MS received 29 November 2022; revised 27 May 2023; accepted 30 May 2023

The altered ultramafic rocks from Higher Himalayan Crystalline (HHC) are characterised by the mineral assemblage of olivine, pyroxene, phlogopite, chromite, and opaques. Olivine and pyroxenes show alteration to serpentine, talc, anthophyllite, and tremolite. In the present research work, the petrogenesis and paleo-tectonic setting of the ultramafic rocks from the Paddar sapphire mining area are understood using chromite chemistry. The investigated chromite is characterised by a higher abundance of Cr₂O₃, FeO, Al₂O₃, and low MgO and is classified as Al-chromite. They show higher Cr# (71.10–87.80) and Fe# (71.66–86.04) and lower Mg# (13.95–28.16), suggesting their affinity towards the ophiolitic peridotite. Chromite geochemistry further suggests that the parent magma originated from the mantle and intruded under high pressure and low oxygen fugacity. Chromite chemistry suggests arc to supra-subduction tectonic setting for the crystallisation of chromite from ultramafic magma. Based on the correlation matrix and binary diagram, it is interpreted that Ti + Cr ↔ Al; Cr ↔ Fe⁺ substitution prevails at the octahedral site, while Fe ↔ Mg; Al ↔ Fe and Al ↔ Mg substitution mechanism operated at the tetrahedral site during the crystallisation of chromite from magma. Further, compositional re-equilibration occurs during hydrothermal alteration.

Keywords. Chromite; ultramafic; peridotite; hydrothermal.

1. Introduction

Chromite [(Mg, Fe²⁺) Cr₂O₄] is one of the end members of the spinel group, represented by the general formula AB₂O₄. While it frequently occurs as an accessory mineral in mafic to ultramafic rocks, it only appears as a dominant mineral in chromitite (Irvine 1965; Rollinson *et al.* 2002). Because it is the first mineral to crystallise from ultramafic magma and a highly sensitive indicator of the primary magma composition, it is frequently utilised as a petrogenetic

indicator (Irvine 1965; Cameron 1975; Zhou *et al.* 2014; Gonzalez-Jimenez *et al.* 2015; Ishwar-Kumar *et al.* 2016; Kang *et al.* 2022). Due to this, many researchers have focused on how the degree of mantle melting, the content of the magma, the order of crystallisation, pressure–temperature parameters, and tectonic context all affect the composition of chromite crystallisation from magma (Barnes and Roeder 2001; Rollinson 2005; Karipi *et al.* 2007; Boudier *et al.* 2021).

The composition of the chromite is controlled by the different processes operating in the magma

chamber like magma differentiation, magma mixing, disequilibrium crystallisation assimilation and cooling rate of magma (Thy 1983; Scowen *et al.* 1991; Yang *et al.* 2021). Dick and Bullen (1984) proposed that $C\#$ increases with the increase of the degree of melting. Bannister *et al.* (1998) demonstrated that continued growth of magnetite on chromite and diffusion in the spinel during cooling of the lava flow gave rise to magnetite, which result in $Cr/Fe^{3+} > 1$ in magnetite while $Fe^{3+}\# (Fe^{3+}/(Cr + Al + Fe^{3+})) > 0.3$ in chromite. Takahashi (1987) recorded that Fo content of the olivine was inversely related to the Ti and $Fe^{3+}\# (Fe^{3+}/(Cr + Al + Fe^{3+}))$ of coexisting chromian spinel phase, while $Cr\# (Cr/(Cr + Al))$ of chromian spinel increases or decreases or is unaffected with a decrease of Fo content of the olivine. However, the composition of the chromite also changes with the grade of metamorphism and hydrothermal alteration (Evans and Frost 1976; Zakrzewski 1989; Kimball 1990).

Many researchers have conducted research on the HHC unit at the regional scale in previous decades. However, the structure, metamorphism, and geochronology were the key areas of attention in their work (Pognante *et al.* 1990; Inger and Harris 1992; Reddy *et al.* 1993; Carosi *et al.* 2010; Webb *et al.* 2011; Thöni *et al.* 2012; Bartoli *et al.* 2019; Carosi *et al.* 2019). Chromite is reported from the ophiolite sequence of Himalayan orogen like Manipur Ophiolite, Nidar Ophiolite, Karzok Ophiolite, Spontang Ophiolite (Nayak and Maibam 2020; Jonnalagadda *et al.* 2022), while chromite chemistry from HHC is rarely reported in published literature along the entire length of Himalayan orogen. Due to the petrogenetic significance of chromite, the present study is an attempt to explore further the importance of detailed petrography and chromite geochemistry in understanding the petrogenesis of ultramafic rocks. Furthermore, we intend to relate the petrogenetic conclusions from investigated chromite. The chromites from the altered ultramafic rocks are investigated for the first time from the Higher Himalayan Crystalline Unit of northwestern Himalaya. The detailed petrological character and geochemistry of chromite are utilised to understand the tectonic setting of parent magma and its post-crystallisation effect.

2. Geological setting

The Himalayas is a typical example of a continent–continent collision orogenic mountain system formed during the Cenozoic period by the collision

between Indian and Eurasian plates that began 55–50 Ma ago (Dewey and Bird 1970; Thakur 1987). The Himalayan orogen is characterised by continuous south-directed thrusting and piling up of tectonic units, traditionally divided into tectonostratigraphic zones (figure 1a), each having characteristic stratigraphy and bounded by major thrust that extends the full length of the orogen (DiPietro and Pogue 2004). Le Fort (1996) divided it from south to north as Neogene Sub-Himalaya (Siwalik Group), the Proterozoic Lesser Himalayan Sequence (LHS), the Proterozoic to Ordovician Greater (or Higher) Himalayan Crystalline Complex (HHC), and the Proterozoic to Eocene Tethyan Himalayan Sequence (THS). But out of these zones, the Higher Himalayan Crystalline (HHC) zone, of which the present area of study is a part, represents the central metamorphic belt and axis of maximum surface uplift of the orogen (Thakur 1980). The HHC is also known as Higher Himalaya/Greater Himalayan Crystalline Complex/Central Himalaya/Central Crystallines. This zone is considered as the backbone of the Himalayan orogen (Saxena 1971) and is characterised by the highest topographical relief. It is commonly represented by a thick Paleoproterozoic to Ordovician (1800–480 Ma) high-grade metamorphic belt and root zone of the allochthonous klippen of the Lesser Himalaya (Parrish and Hodges 1996; DeCelles *et al.* 2000). These metasediments are frequently intruded by granites of Ordovician (~500 Ma) and Lower Miocene (~22 Ma) age.

Geologically, the study area is part of the Kishtwar region, which shows a very complex litho-tectonic setup as it is surrounded by Kashmir Nappe in the west; where the THS directly overlies the LHS along the MCT (Frank *et al.* 1995; Pogue *et al.* 1999). The present investigation is confined to the Paddar Sapphire mine area, exposing the high-grade metamorphic rock of the HHC unit of Himalayan orogen. In general, the stones of HHC rocks show thrust contact with Lesser Himalaya marked by the well-known Main Central Thrust (MCT, figure 1b). The low-grade metamorphic rocks of Lesser Himalayan form window structure (Kishtwar Window) within HHC along the Kishtwar Fault (Fuchs 1975; Stephenson *et al.* 2000; Singh 2010). The Zaskar Shear Zone (ZSZ) marks the boundary between HHC and Tethys Himalaya along the northern edge of the HHC (Herren 1987; Singh 2010). Precambrian HHC occurs at the base of Tethys Himalaya, forming the basement (Thakur 1987).

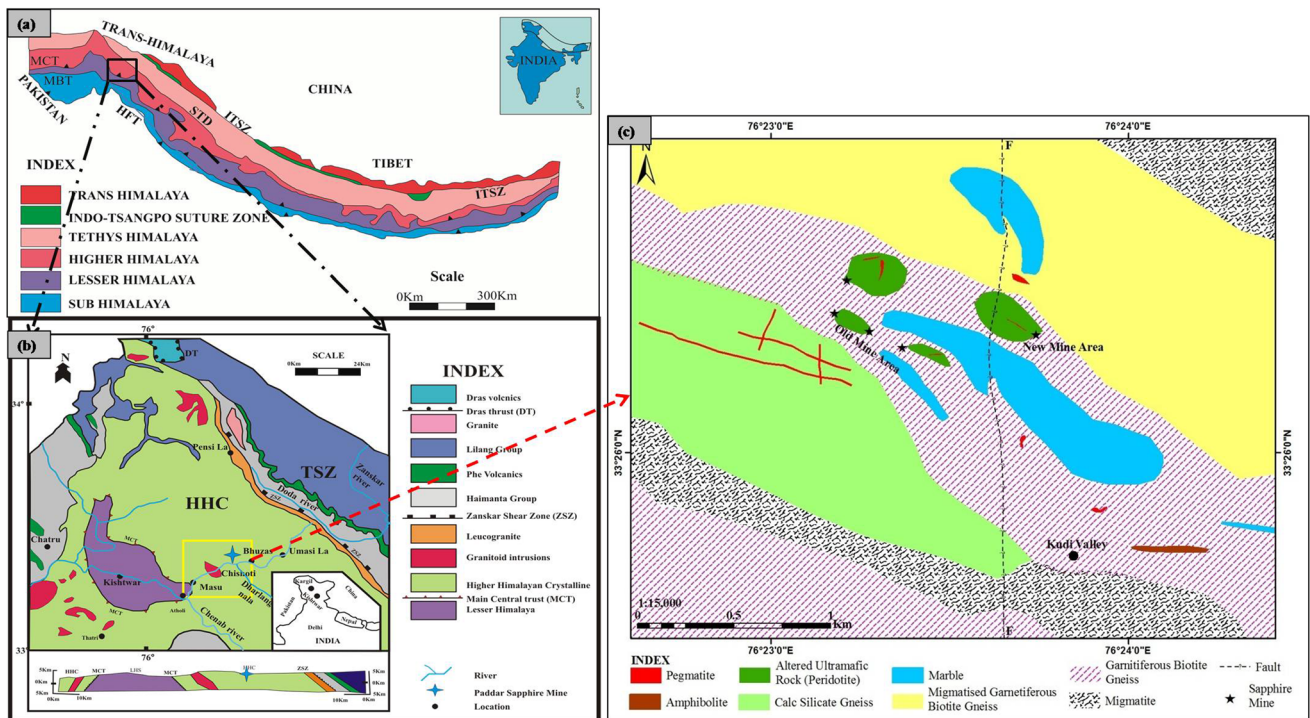


Figure 1. Geological setup of the study area. (a) Tectonic subdivision of Himalaya marked by thrust system and (b) regional geological map of the study area (after Sorkhabi *et al.* 1997). ITSZ: Indo-Tsangpo Suture Zone, STD: South Tibetan Detachment, MCT: Main Central Thrust, MBT: Main Boundary Thrust, HFT: Himalayan Frontal Thrust. (c) Geological map of Paddar sapphire mine area showing the distribution of pegmatites (after Srivastava and Singh 2022).

In the present study area, HHC is composed of migmatites, gneisses of sedimentary protolith associated with gneisses of magmatic protolith, pelitic schists, intruded by porphyritic granites and leucogranites (Stephenson *et al.* 2000; Singh 2010). The Tethys Himalaya of the Paleozoic–Mesozoic age is represented by a thick marine sedimentary sequence intruded by Permian volcanic (e.g., Frank *et al.* 1995). In the Paddar area, the Lesser Himalayan unit is represented by quartzites, phyllites, slate, schist, mylonitic augen gneiss, volcanics, and gneissose granite. The western and southern boundaries of the Kishtwar Window are represented by the sericitic-phyllites and quartzites and show a gentle dip towards N to NE (Fuchs 1975; Honegger 1983; Staubli 1988). Tewari (1981) proposed gneissic rocks intercalated with marble occur as exotic thrust mass placed over migmatitic complex, as a klippe along Sumjum Thrust. Singh (2007) classified the stones of the proterozoic rocks of Lesser Himalaya and HHC under the Kishtwar Group. In the Kishtwar region, the Phe Formation, Haimanta Group, and the Lilang Group are exposed in the north of the HHC.

The Kishtwar region has undergone three phases of metamorphism represented by M1 (amphibolites grade metamorphism with moderate pressure), M2

(development of syn-metamorphic dome in the Higher Himalaya), and M3 (retrogressive mineral assemblage quartz–muscovite–chlorite and the upliftment of the Kishtwar window; Kundig 1989; Staubli 1989; Frank *et al.* 1995; Stephenson *et al.* 2000). The M2 phase is associated with the migmatitisation and large-scale crustal melting in the HHC (Noble and Searle 1995). Kundig (1989) observed several gneisses domes, such as the Chishoti dome and the Bhazun dome, at the lower structural level within the HHC unit just north of the Kishtwar window. These domes are syn-metamorphic in origin and consist of pelitic schists and gneisses folded around granite and granitic gneiss core. Migmatitisation commonly occurs along the contacts within the granites and overlying schists and gneisses. In Bhat Nala, folding of the main foliation into the adjacent Chisoti and Bhazun domes creates foliation triple junctions. These suggest regions of high strain and are characterised by isoclinal folded compositional banding into upright-facing synforms. Stephenson *et al.* (2001) interpreted it as synchronous with thrusting on the Main Central Thrust and local extension on the Zaskar Shear Zone. Searle *et al.* (2007) also suggested that the domes were synchronous with movement on the Main Central Thrust and could be thrust-related culminations. Fission

track data, however, from the cores of the Chisoti dome suggests that these structures have experienced relatively fast exhumation (Kumar *et al.* 1995).

3. Sampling and analytical technique

The author carried out detailed fieldwork in the HHC of the Paddar area along the Bhat Nala. About 30 samples of ultramafic rock were selected for detailed petrographic examination. Based on the petrography, three samples were selected for the EPMA investigation to better understand the compositions of the opaque mineral phase. At the Department of Geology, Banaras Hindu University, the chosen chromite grains are examined using the Electron Probe Micro Analyzer (EPMA) CAMECA SXFive. For performing the analysis, the polished thin sections were coated with a 20 nm thin layer of carbon by using the LEICA-EM ACE200 instrument. The instrument was operated at a voltage of 15 kV with 40 nA and set with a focused beam of diameter 1 μm with counting time of 120 to 300 seconds. B–K, Na–K, Mg–K, Al–K, Si–K, K–K, Ca–K, Ti–K, Cr–K, and Fe–K X-ray lines were employed in the analysis. For calibration, a variety of synthetic and natural standards were used. For major element oxides, the analysis accuracy is better than 1%. The representative compositions of chromite grains along with the calculated mineral formula based on 32 oxygen atoms, are given in table 1.

4. Field description and petrography

The ultramafic rocks are the conspicuous rock in the study area. The fresh rock shows an olive-green hue, while the weathered surface of these rocks has an oxidised brown staining. They are intruded in the gneissic rocks in the form of small bodies of laccolith, lenses, and bulbous (figure 2). They contain olivine and pyroxenes predominately, along with varying amounts of opaque minerals. They are intensely altered to serpentine and talc, giving a soapy feel while touching with a hand. They are enclosed within the garnetiferous biotite gneiss and shows both concordant and discordant relationship. They show forceful emplacement by the up arching of the strata is clearly visible in the main sapphire mine ridge (figure 2).

The ultramafic rocks are the most interesting rock types well exposed in the Paddar sapphire mine area. They are medium to coarse-grained, characterised by radiating crystals of pyroxenes and amphiboles. Mineralogical composed of olivine and pyroxene as

main mineral phases while phlogopite and opaque minerals occur as minor mineral phases (figure 3). The main mineral phases (olivine + pyroxene) show alteration to talc, serpentine, anthophyllite, and tremolite by the effect hydrothermal fluids (figure 3).

Fe-oxide and chromite are the opaque phases identified in EPMA studies. Chromite is one of the most important accessory phases in these rocks. They occur as isolated subhedral to anhedral grains and scattered fine dust in altered parts (figure 4a, b). They vary in size from <5 to 800 μm in diameter. They occupy the intergranular space between olivine, pyroxene, and altered domain (figure 4c). Some subhedral grains have sharp boundaries with phlogopite and pyroxenes. Most of the grains are unaltered and homogenous, except the grain boundary is corroded (figure 4c, d). However, some grains show alteration along the fractures (figure 4d).

5. Chromite chemistry

The chromite from the ultramafics of the study area shows enrichment and a wide range of Cr_2O_3 and Al_2O_3 ranging from 47.89 to 60.18 wt%, 5.57–13.40 wt% with an average of 56.38 wt%, 8.53 wt%, respectively. The FeO is also higher in concentration, but it is more consistent ranging from 22.10 to 28.98 wt% with an average of 25.65 wt%. However, the MgO is lower in concentration, varying from 2.58–5.49 wt% with an average of 4.36 wt%. The Na_2O and K_2O occur in traces <0.1%. The CaO is higher than the alkali elements ranging from 0.002 to 0.21 wt% with an average of 0.06 wt%.

The TiO_2 varies from 0.03 to 0.72 wt%, which is higher in concentration, while MnO is detected in a few analysed points ranging from 0.43 to 0.66 wt%. The P_2O_5 varies from 0.01 to 0.13 wt% and chlorine content ranges from 0.0010 to 0.02 wt%.

The chromites show very higher Cr# ($100 \cdot \text{Cr} / (\text{Cr} + \text{Al})$), ranging from 71.10 to 87.80 with an average of 81.55. However, they show wider ranges of the Mg# ($100 \cdot \text{Mg} / (\text{Mg} + \text{Fe}^{2+})$) ranging between 13.95 and 28.16 with an average of 23.36, while Fe^{3+} # ($100 \cdot \text{Fe}^{3+} / (\text{Cr} + \text{Al})$) varies in a range of <0.1–2.15.

6. Discussion

6.1 Classification of chromite

Based on structure, Palache *et al.* (1944) divided the spinel group into three series: the spinel series, magnetite series, and chromite series. According to

Table 1. Representative electron microprobe analysis (in wt%), cation proportion and composition of chromite from altered ultramafic rocks of Paddar area.

Sample points	31	32	33	34	35	76	77	78	79	80	81	82	83
Cr ₂ O ₃	59.39	60.18	59.07	58.70	54.87	59.84	59.27	58.71	58.36	57.09	47.90	49.18	50.47
Al ₂ O ₃	7.83	7.92	7.32	7.90	11.48	5.57	6.68	6.58	6.17	7.92	10.33	13.40	11.87
TiO ₂	0.66	0.69	0.72	0.15	0.19	0.34	0.39	0.41	0.04	0.06	0.04	0.11	0.13
FeO	24.14	24.69	25.23	25.36	26.10	25.31	25.30	25.61	25.95	26.76	22.11	27.93	28.99
MgO	4.71	5.49	4.24	3.46	4.16	4.32	5.34	5.41	4.25	4.09	4.63	4.11	2.58
MnO	0.61	0.60	0.67	0.50	0.44	0.00	0.00	0.00	0.00	0.00	0.00	0.00	0.00
Total	97.34	99.57	97.26	96.08	97.23	95.39	96.99	96.72	94.77	95.92	85.00	94.73	94.04
Formula units based on 32 oxygen and Fe ²⁺ /Fe ³⁺ assuming full site occupancy													
Cr	13.38	13.19	13.40	13.51	12.21	13.92	13.40	13.30	13.62	13.08	12.07	11.10	11.69
Al	2.63	2.59	2.48	2.71	3.81	1.93	2.25	2.22	2.15	2.71	3.88	4.51	4.10
Ti	0.14	0.14	0.16	0.03	0.04	0.08	0.08	0.09	0.01	0.01	0.01	0.02	0.03
Fe ³⁺	0.00	0.00	0.00	0.00	0.00	0.00	0.19	0.30	0.21	0.19	0.03	0.34	0.15
Fe ²⁺	6.05	5.79	6.24	6.47	6.25	6.24	5.86	5.84	6.20	6.30	5.86	6.32	6.95
Mg	2.00	2.27	1.81	1.50	1.74	1.90	2.28	2.31	1.87	1.77	2.20	1.75	1.13
Mn	0.09	0.08	0.10	0.07	0.05	0.00	0.00	0.00	0.00	0.00	0.00	0.00	0.00
Ni	0.00	0.00	0.00	0.00	0.00	0.00	0.00	0.00	0.00	0.00	0.00	0.00	0.00
Total	24.00	24.00	24.00	24.00	24.00	24.00	24.00	24.00	24.00	24.00	24.00	24.00	24.00
Al ₂ O ₃ in melt	9.35	9.39	9.09	9.38	10.95	8.12	8.75	8.70	8.47	9.39	10.48	11.67	11.10
Fe ²⁺ /Fe ³⁺	0.00	0.00	0.00	0.00	0.00	0.00	31.62	19.62	29.39	34.00	212.05	18.38	46.10
100Mg/Mg+Fe ²⁺	23.04	27.09	20.81	16.37	17.34	23.20	28.05	28.63	22.41	19.63	22.54	16.15	10.20
100Cr/Cr+Al	83.57	83.60	84.40	83.28	76.23	87.81	85.61	85.67	86.38	82.86	75.66	71.10	74.04
100Fe ³⁺ /Cr+Al+Fe ³⁺	0.00	0.00	0.00	0.00	0.00	0.00	1.17	1.88	1.32	1.16	0.17	2.16	0.95
Fe ³⁺ /Fe ²⁺	0.00	0.00	0.00	0.00	0.00	0.00	0.03	0.05	0.03	0.03	0.00	0.05	0.02
Cr/Cr+Al	0.84	0.84	0.84	0.83	0.76	0.88	0.86	0.86	0.86	0.83	0.76	0.71	0.74
Mg#	0.25	0.28	0.23	0.19	0.22	0.23	0.28	0.28	0.23	0.22	0.27	0.22	0.14
Fe ²⁺ #	0.75	0.72	0.77	0.81	0.78	0.77	0.72	0.72	0.77	0.78	0.73	0.78	0.86

guidelines of nomenclature and Commission on New Minerals, Nomenclature and Classification (CNMNC), Mills *et al.* (2009) classified the spinel supergroup into three groups on the basis of the X species given in table 2. The chromite mineral series are classified under the spinel subgroup (2–3) represented by the general formula A²⁺(B³⁺)₂O₄ under the Oxyspinel group. Naturally, occurring chromites are essentially solid solutions mainly of the Mg and Fe members of the spinel and chromite series, viz., magnesiochromite and (ferro) chromite, with minor amounts of the magnetite series. On plotting the composition of analysed mineral grain in Cr–Al–Fe³⁺ ternary classification diagram (after Stevens 1944), all grains occupy the Al-chromite field.

The spinel prism (figure 5a) diagram, presented by Haggerty (1991), represents a solid solution between spinel, hercynite, chromite, magnesiochromite, magnesioferrite, and magnetite. Gargiulo *et al.* (2013) projected the face ‘B’ and ‘C’ of the prism diagram into compositional variation

diagrams based on the previously published diagrams of Stevens (1944) and Deer *et al.* (1992).

On plotting the composition of analysed chromite in ternary Y(Cr³⁺) = Cr/(Cr + Fe³⁺ + Al); Y(Fe³⁺) = Fe³⁺/(Cr + Fe³⁺ + Al); Y(Al³⁺) = Al/(Cr + Fe³⁺ + Al) diagram the analysed points occupy the Al-chromite to chromite field (figure 5b). Further, in both classification diagrams, the chromite displays Cr–Al trend indicating Cr ↔ Al substitution. On the projected ‘C’ face of the spinel prism diagram in binary Mg²⁺/Mg²⁺ + Fe²⁺ vs. Al³⁺/Fe³⁺ + Al³⁺ plot, most of the analysed chromites fall in the spinel field while few fall in the pleonaste field (figure 5c). From this plot, it is evident that in the X-site shows, there was lower Mg²⁺–Fe²⁺ and Al³⁺–Fe³⁺ exchange during the crystallisation. Further on plotting the Cr number and Mg number of the studied chromite in the Mg²⁺/Mg²⁺ + Fe²⁺ vs. Cr/Al + Cr, all the analysed points are occupying chromite field, indicating higher chromium and iron concentration as compared to the magnesia (figure 5d).

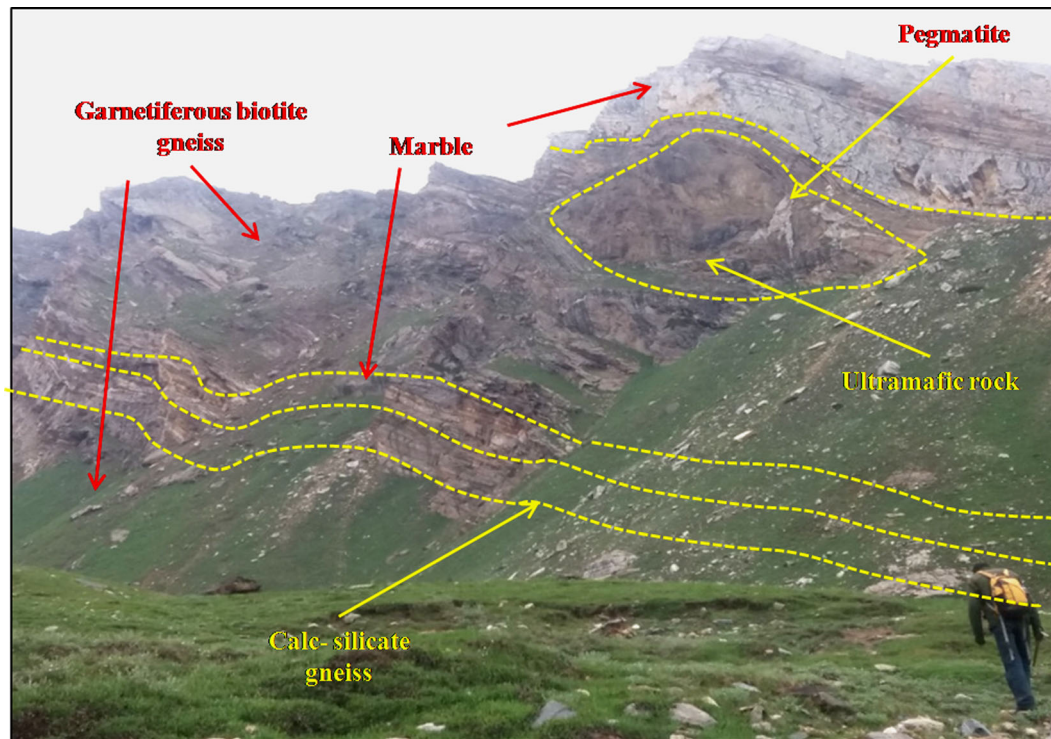


Figure 2. Regional view of sapphire mine ridge showing ultramafic rock intruded into garnetiferous biotite gneiss, up arched marble bed at the top of the ridge.

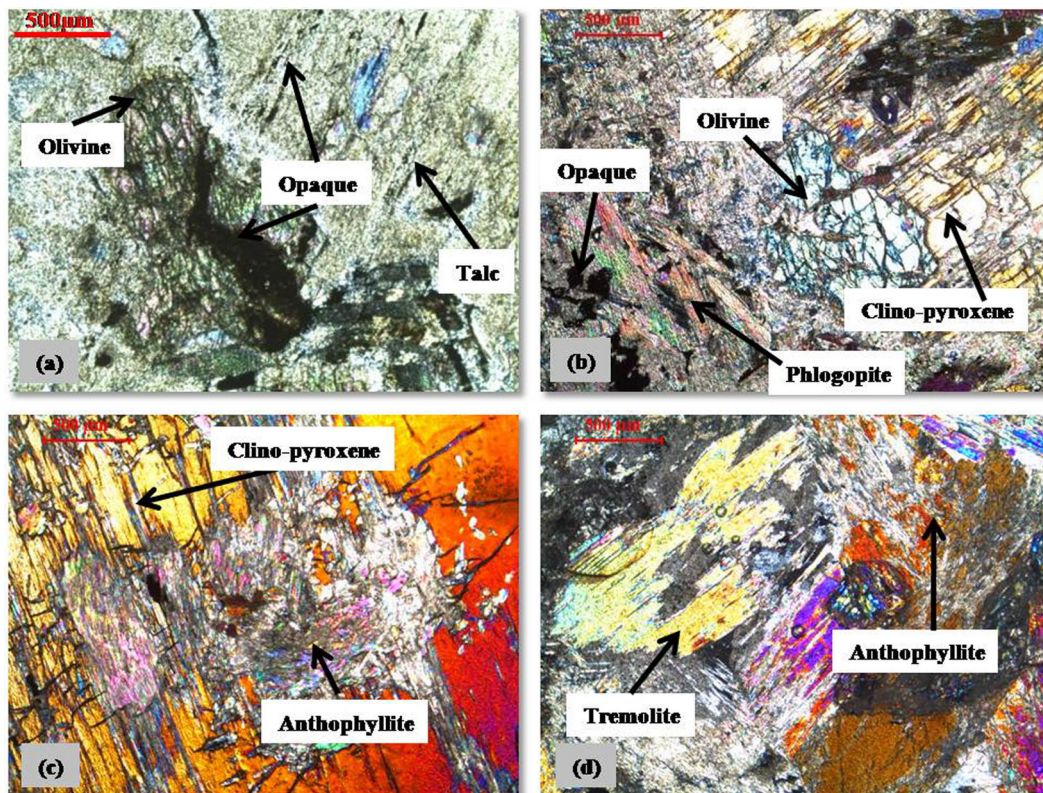


Figure 3. (a) Relict olivine grain associated with opaque mineral and surrounded by talc alteration. (b) Serpentinised olivine grain sharing grain boundary with clinopyroxene, phlogopite, opaque minerals are also present. (c) Clinopyroxene altered to anthophyllite. (d) Pyroxene and olivine altered to tremolite and anthophyllite.

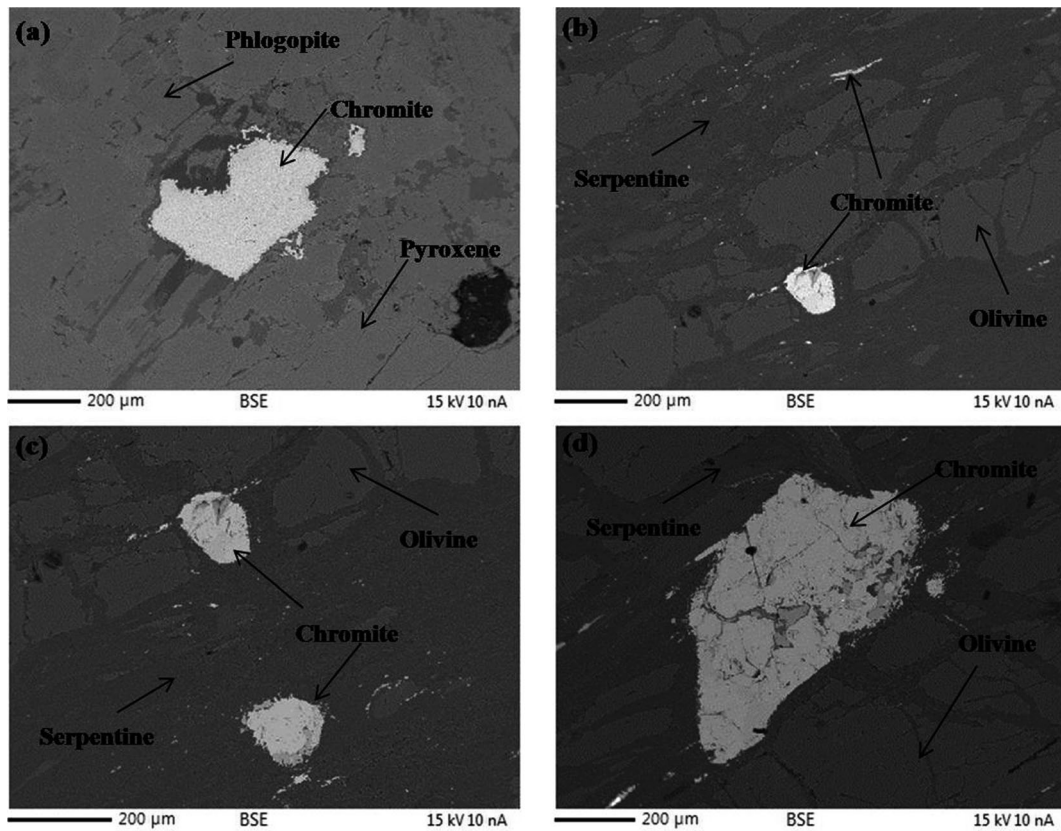


Figure 4. (a) Chromite grain sharing boundary with phlogopite and pyroxene, grain boundary of chromite is corroded due to alteration, (b) chromite showing variation in the grain size, (c) chromite grains associated with serpentinised olivine grain, and (d) subhedral chromite grain altered along the fracture and grain boundary.

Table 2. The classification of the spinel supergroup into group-subgroup hierarchy and general formulae of the spinels (Mills et al. 2009).

Supergroup	Group	Subgroup	General formula
Spinel supergroup	Oxyspinel group	Spinel subgroup (2-3)	$A^{2+} (B^{3+})_2O_4$
		Ulvospinel subgroup (4-2)	$A^{4+} (B^{2+})_2O_4$
	Thiospinel group	Carrollite subgroup (1-3-5)	$A^{1+} (B^{3.5+})_2S_4$
		Linnaeite subgroup (2-3)	$A^{2+} (B^{3+})_2S_4$
	Selenospinel group	Tyrrellite subgroup (1-3-5)	$Mg\# (Mg+Fe/Mg)$
		Bornhardtite subgroup (2-3)	$Fe^{2+\#} (Fe+Mg/Fe)$

6.2 Substitution mechanism

The spinel group is represented by the general formula AB_2X_4 , here A and B represent the constituents instead of the crystallographic site. The octahedral site in the chromite is occupied by Cr, which is substituted by trivalent and tetravalent cations such as Al^{3+} , Fe^{3+} , Ga^{3+} , Sc^{3+} , V^{3+} , and Ti^{4+} . The tetrahedral site is mainly occupied by Mg and Fe^{2+} that may be substituted by divalent

cations Zn, Co, Mn, and Ni. The correlation matrix of the major and minor elements is presented in table 3. The binary variation diagram of the cations per unit formula shows significant positive (+ve *R*-value) and negative relation (-ve *R*-value) between the elements. The Cr shows a strong negative relationship with the Al with a very high *R*-value of -0.98, while it shows significant positive relation with Ti (*R* = 0.46). However, the Al shows negative relation with the Ti with a -0.46 *R*-value.

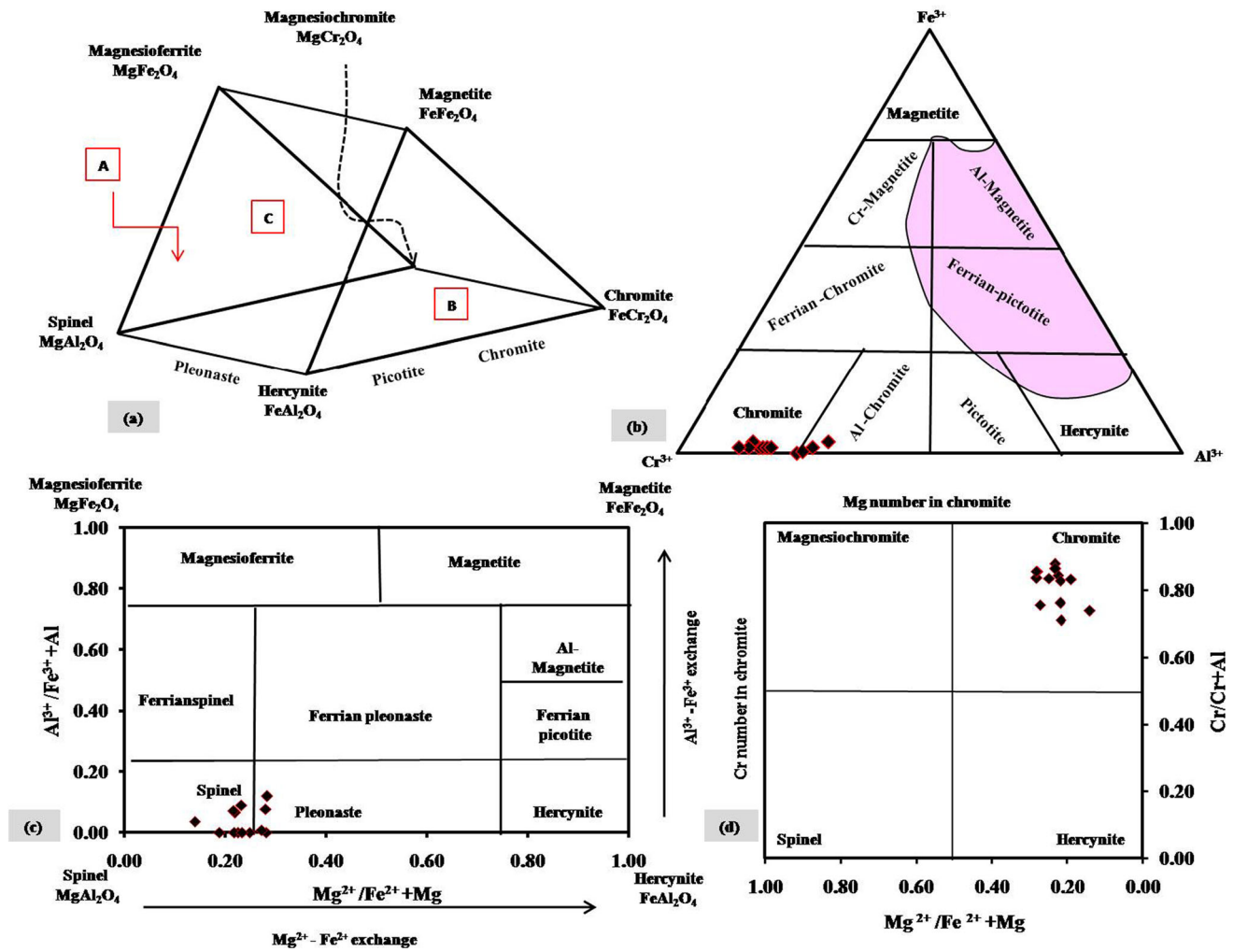


Figure 5. Chemical classification diagrams for the chromite from Paddar area. (a) Spinel prism for the multi-component system: spinel–hercynite–chromite–magnesiocromite–magnesioferrite–magnetite (after Deer *et al.* 1992); (b) Triangular classification diagram (Cr^{3+} – Fe^{3+} – Al^{3+}): $Y(Cr^{3+}) = Cr/(Cr + Fe^{3+} + Al)$; $Y(Fe^{3+}) = Fe^{3+}/(Cr + Fe^{3+} + Al)$; $Y(Al^{3+}) = Al/(Cr + Fe^{3+} + Al)$. Spinel gap field from Barnes and Roeder (2001). (c) Binary classification diagram considering the Mg^{2+} – Fe^{2+} exchange in the structural site ‘X’: $Fe^{2+}/(Mg^{2+} + Fe^{2+})$. (d) Classification diagram for chromites in terms of Mg number [$Mg^{2+}/(Mg^{2+} + Fe^{2+})$] vs. Cr-number [$Cr/(Cr + Al)$]. Fields are after Kapsiotis (2009).

Table 3. Pearson correlation matrix of major and minor elements for investigated chromite.

	Cr	Al	Ti	Fe^{3+}	Fe^{2+}	Mg	Mn	Fe_t
Cr	1							
Al	–0.98	1						
Ti	0.44	–0.46	1					
Fe^{3+}	–0.34	0.17	–0.39	1				
Fe^{2+}	–0.35	0.41	–0.41	0.04	1			
Mg	0.36	–0.44	0.41	0.04	–0.99	1		
Mn	0.28	–0.16	0.72	–0.67	–0.11	0.014	1	
Fe_t	–0.45	0.44	–0.52	0.40	0.93	–0.891	–0.35	1

The Fe^{3+} shows negative relation with the Cr ($R = -0.34$) and Ti ($R = -0.39$; figure 6). Based on these relations, it is suggested that $Ti + Cr \leftrightarrow Al$

and $Cr \leftrightarrow Fe$ substitution mechanism operated in the octahedral site. The binary variation diagram (figure 7) shows a strong negative relation between

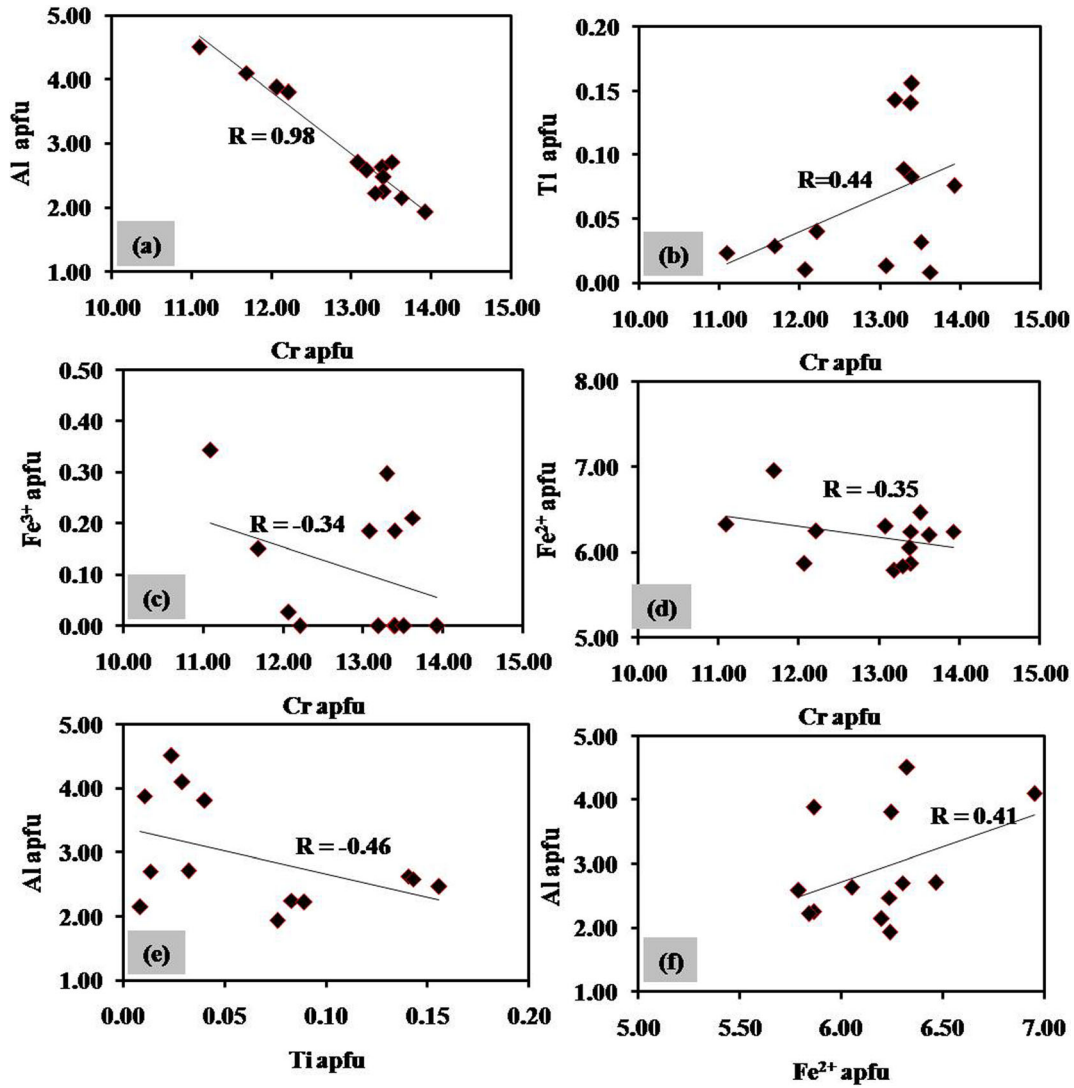


Figure 6. Binary variation diagram of major and minor elements to understand the substitution mechanism in the chromite during its crystallisation: (a) Al vs. Cr; (b) Ti vs. Cr; (c) Fe³⁺ vs. Cr; (d) Fe²⁺ vs. Cr; (e) Al vs. Ti; (f) Al vs. Fe²⁺. Note: Al, Fe³⁺ and Fe²⁺ show antipathic relationship with Cr, while Ti shows sympathetic relationship (a–d). Further, antipathic relationship is observed between Al and Ti, while Al shows sympathetic relationship with Fe²⁺. Scattering of the elements is due to the hydrothermal alteration.

the Fe²⁺ and Mg ($R = -0.99$) while positive relation of Mg with Ti ($R = 0.41$). However, Al shows negative relation with both Fe²⁺ and Mg. Thus it is evident that Fe ↔ Mg and Al substitute both Fe and Mg in the tetrahedral site.

6.3 Metamorphism and alteration effect

Chromite re-equilibration, hydrothermal alteration, and metamorphic modification have all been extensively covered in previous research (Onyegocha 1974; Ulmer 1974; Evans and Frost 1976; Hoffman and Walker 1978; Loferski and Lipin 1983; Kimball 1990; Burkhard 1993). These

investigations show that chromite alteration results in the overgrowth of magnetite rim and is gradually replaced by chromian magnetite, also known as ‘ferritchromite’. By exchanging components with nearby silicate minerals, the prograde metamorphism (green-schist to amphibolite facies) modifies the core-to-rim compositional zoning (Evans and Frost 1976; Abzalov 1998; Barnes 2000; Gonzalez Jimenez *et al.* 2009; Waterton *et al.* 2020). Previous investigations of chromite chemistry suggest that alteration and post-crystallisation re-equilibration leads to the complexity of the interpretation (Evans and Frost 1976; Burkhard 1993).

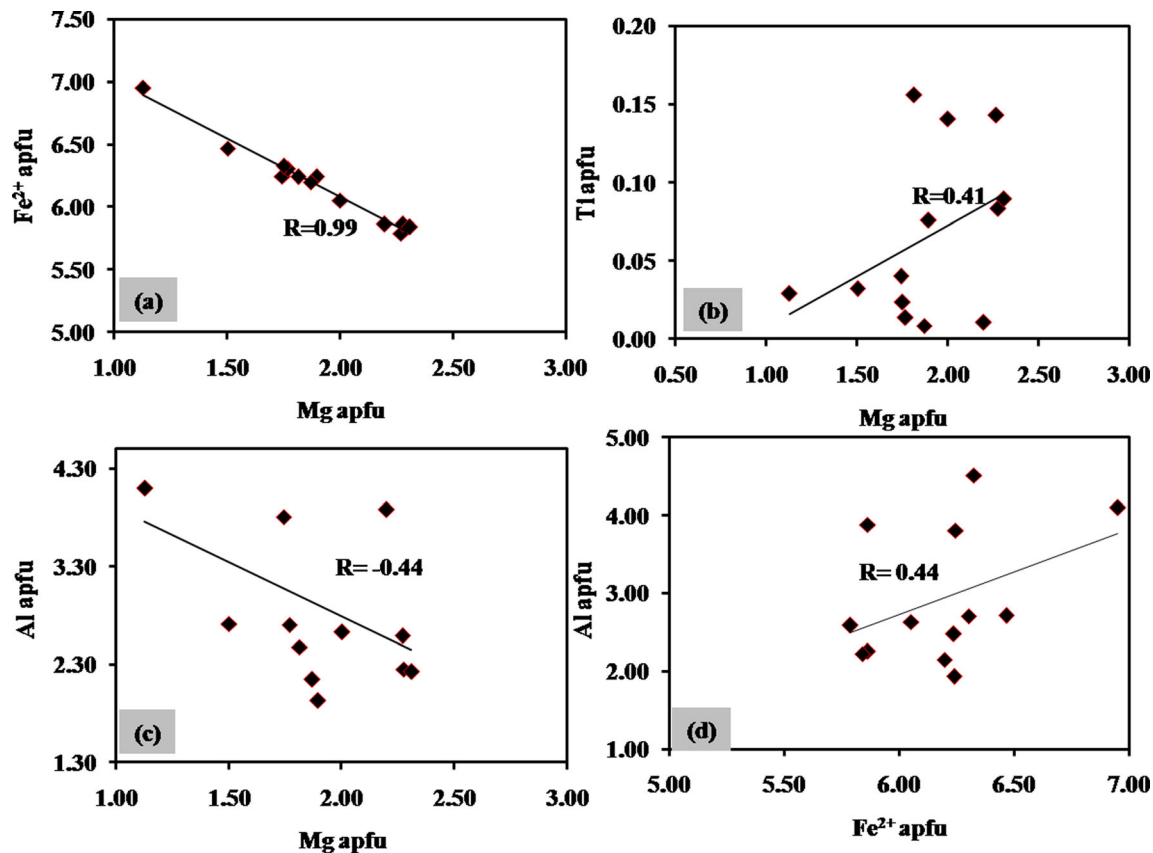


Figure 7. Binary variation diagram of major and minor elements to understand the substitution mechanism in the chromite during its crystallisation: (a) Fe^{2+} vs. Mg; (b) Ti vs. Mg; (c) Al vs. Mg and (d) Al vs. Fe^{2+} . Note: Fe^{2+} and Al show antipathic relationship with Mg, while Ti shows sympathetic relationship and a sympathetic relationship is observed between Ti and Mg.

The metamorphic transformation is well recovered as optical and compositional zoning of chromite. However, some authors believe that optical zoning is completely eradicated during the prograde metamorphism at a higher grade of metamorphism that gives rise to ferrian chromite or Cr-magnetite and/or with a homogenous chemistry (Ulmer 1974; Barnes 2000; González Jiménez *et al.* 2009).

The petrographic study of the chromite from the study area reveals that chromites are homogenous and do not show any optical zoning. However, the alteration of these chromites is confirmed by the alteration observed along the fractures and corroded grain boundary. This is well reflected in the BSE images (figure 4). To observe the effect of metamorphism/alteration on chromite, different plots are used. On plotting the chromite chemistry in $\text{Fe}\#$ vs. $\text{Mg}\#$ diagram (figure 8a), the investigated chromite falls near the partly altered chromite field. From this plot, it is revealed that these chromite grains have depleted Fe^{3+} and Mg content. On plotting the chemistry of the chromite in $\text{Mg}\#$ vs. $\text{Cr}\#$ diagram (figure 8b), they are showing $\text{Cr}\#$ within range of the

partly altered chromite while depleted Mg content. Further on plotting the chromite chemistry in the ternary Cr–Al– Fe^{3+} diagram (figure 8c), it is confirmed that chromite from the Paddar area has undergone the effect of metamorphism/alteration. Most of the investigated chromite falls near the spinel core field, and some occupy the spinel core field in $\text{Cr}\#$ vs. $\text{Fe}^{3+}\#$ diagram (figure 8d), which does not follow the typical alteration trend of Fe^{3+} enrichment. From the above discussion, it is inferred that chromite grains are suitable for petrogenetic investigation. Liipo *et al.* (1994) observed low X_{Mg} (0.0–0.37) and revealed that Mg and Al are more mobile than Cr during the hydrothermal alteration. Similar results were recorded by Kimball (1990). The depletion of Mg and Al content of the chromite from the present study area can be related to the hydrothermal alteration.

6.4 Composition and environment of the parent magma

Primary chromite phases' composition is closely related to the composition of the parental melt, the

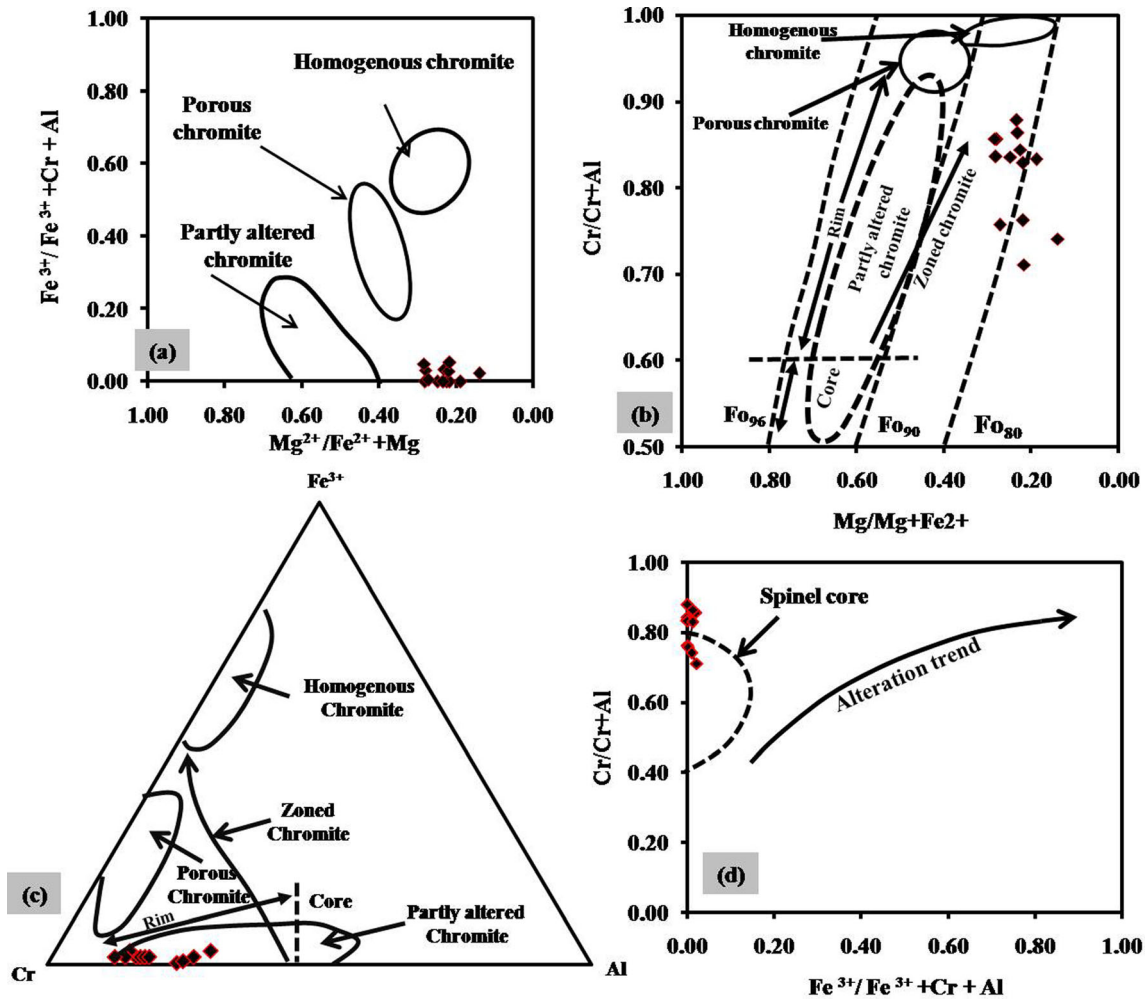


Figure 8. (a) Fe# vs. Mg# diagram, (b) Mg# vs. Cr# diagram, (c) ternary Cr–Al–Fe³⁺ diagram, and (d) the Cr# [Cr/(Cr + Al)] vs. Fe³⁺# [Fe³⁺/(Cr + Al + Fe³⁺)] plot defining the unaltered nature chromites from the study area (modified after Ahmed *et al.* 2009).

extent of partial melting, and the fractional crystallisation, thus effectively used by many workers to measure parental melt composition (Irvine 1977; Barnes and Roeder 2001). The aluminum concentration in chromite is fruitful for the study of the tectonic environment and the melt composition (Zhou *et al.* 1996; Rollinson 2008; Zaccarini *et al.* 2011). In 1982, Maurel and Maurel proposed the equation $[Al_2O_3]_{spinel} = 0.035 \times (Al_2O_3)_{melt}^{2.42}$ for the estimation of the alumina in the parent magma by considering the equilibrium between melt and chromite at 1 Kb. According to the equation, the calculated Al₂O₃ of the parent melt in which the chromite of the study area varies from 8.11 to 11.67 wt% (table 1).

In order to interpret the crystallisation pressure of ultramafic rocks, Basu and McGregor (1976) observed significant variation in the Mg# and Cr# in the chromite from alkali-basalt and kimberlite xenoliths. As a result, he proposed that this

relationship between the Mg# and Cr# in the chromite is appropriate. Using these parameters by plotting the studied chromites in the Mg# (Mg²⁺/Mg²⁺ + Fe²⁺) vs. Cr# (Cr/(Cr + Al)) plot, the chromites from the study area show higher Cr# while lower Mg# thus fall near the field of chromites from the Kimberlite xenoliths suggesting that these chromites crystallised at high pressure (figure 9a). The Fe³⁺/Fe²⁺ ratio is <0.05, suggesting chromite crystallisation at low oxygen fugacity.

6.5 Petrogenetic implications

Due to chromite’s sensitivity to the parent magma/melt composition and its early crystallisation from mafic–ultramafic magma, it has been employed extensively to study the petrogenesis of its host rocks (Irvine 1965; Cameron 1975; Barnes

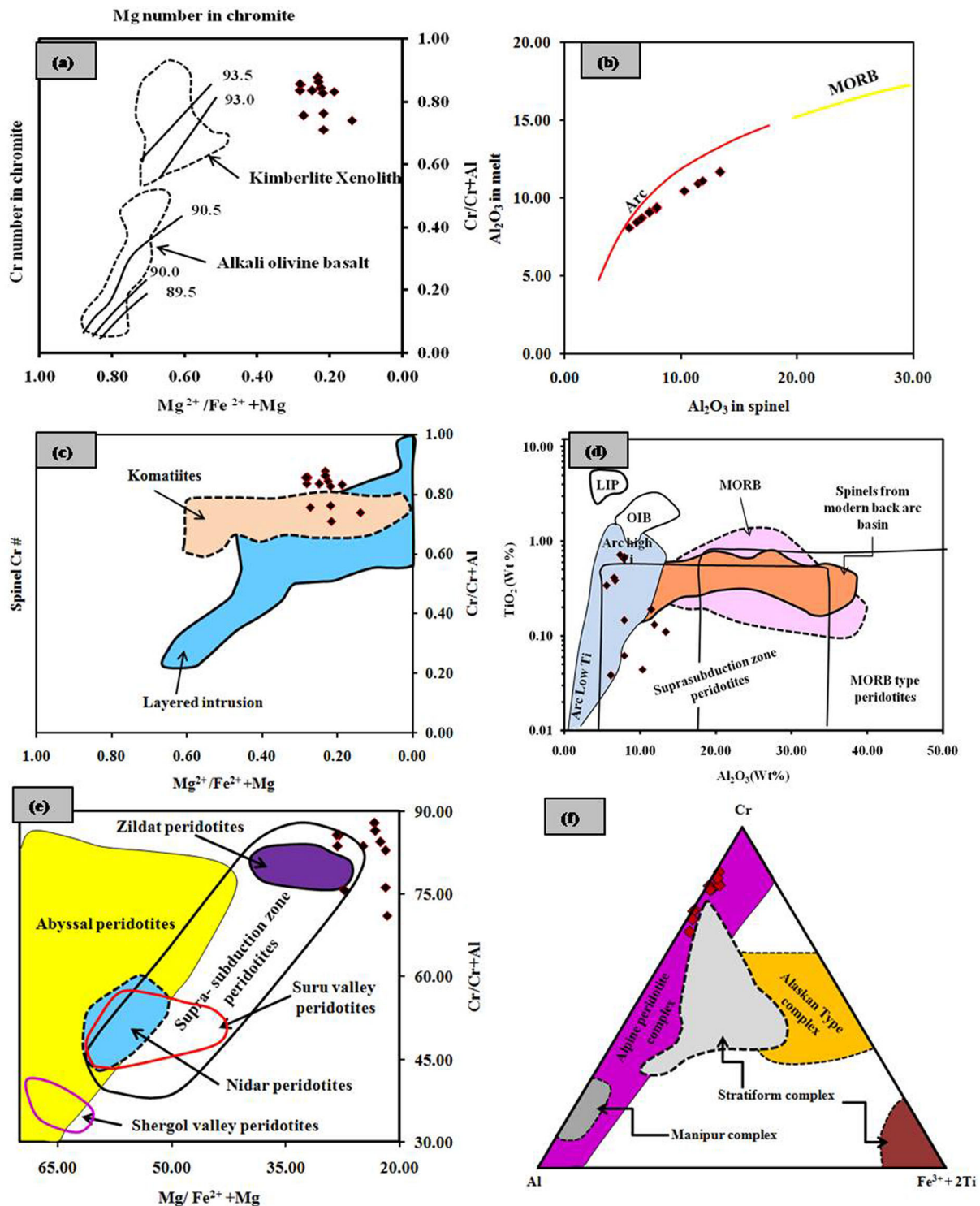


Figure 9. Discrimination diagrams (a) Cr# vs. Mg# diagram showing the discrimination between alkali-basalt and kimberlite xenoliths (after Basu and McGregor 1975). The chromites from the Paddar area falls near the kimberlite xenolith field, suggesting a high-pressure origin; (b) Plot based on the estimated composition of parental magma, Al₂O₃ in melts vs. Al₂O₃ in spinel (after Rollinson 2008), based on melt calculations of Maurel and Maurel (1982); (c) Cr# vs. Mg# plot showing discrimination between chromites from Komatiites and layered intrusion (fields after Barnes and Roeder 2001), studied chromites shows affinity towards komatiite; (d) Tectonic discrimination diagram based on TiO₂ vs. Al₂O₃ for chromite from Paddar area (fields after Kamenetsky *et al.* 2001) indicating arc to supra-subduction tectonic setting; (e) Plot of Mg# against Cr# showing compositions of chromite from Paddar ultramafics in comparison to various ophiolite rocks. Cr-spinel compositional fields of Zildat and Nidar peridotites are from Guillot *et al.* (2001), Shergol and Suru valley peridotites are from Bhat *et al.* (2019), abyssal peridotite is from Dick and Bullen (1984) and supra-subduction zone peridotite is from Ishii (1992); (f) Ternary Cr–Al–Fe³⁺+2Ti plot, the investigated chromite occupy field of alpine peridotite complex (field after Jan and Windley 1990; Zhou and Kerrich 1992).

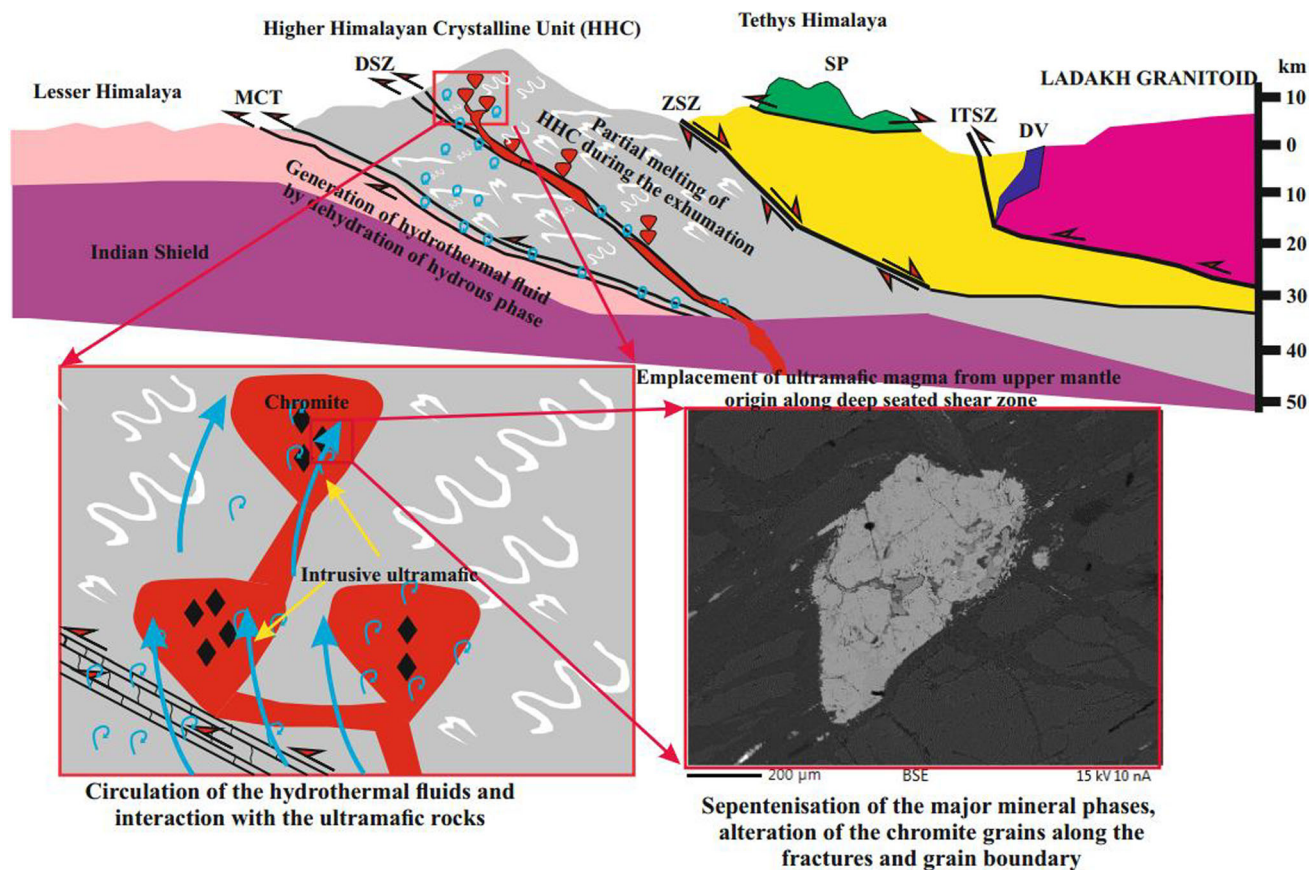


Figure 10. Schematic tectonomagmatic model for the formation of chromites in ultramafics of Higher Himalayan Crystalline Unit (HHC) in the NW Hiamalyan orogen belt and alteration of chromite by hydrothermal fluids generated along the shear zones. Abbreviation: MCT: Main Central Thrust, DSZ: Darlang Shear Zone, ZSZ: Zanskar Shear Zone, SP: Spotang Ophiolite, ITSZ: Indus-Tsangpo Suture Zone, DV: Dras Volcanics (Kishtwar-Western Zanskar cross-section after Searle *et al.* 2007).

and Hill 1995; Zhou *et al.* 2014; Ishwar-Kumar *et al.* 2016). In podiform chromitites, a wide variety of compositions were noted by Saleh (2006). They are characterised by high Cr (0.62–0.88) to high Al varieties. The chromites from ophiolites are high-Cr and high-Al. High-Al chromitites evolve from basaltic melts in a back-arc basin or MORB environment, whereas high-Cr chromitites develop from andesitic or boninitic melts that are Mg-rich (e.g., Zhou and Robinson 1994; Arai 1997; Zhou *et al.* 1998; Akmaz *et al.* 2014; Moghadam *et al.* 2015). Alaskan-type complexes are distinguished from ophiolitic or stratiform complexes by their higher Fe^{3+} and Ti contents and lower Al contents (Bird and Clark 1976). Arc environments are characterised by Cr-rich spinels ($Cr\# > 0.7$), whereas MOR settings are characterised by Cr-poor spinels ($Cr\# 0.6$; e.g., Zhou *et al.* 1998; Kamenetsky *et al.* 2001). In order to understand the petrogenesis of the ultramafic of Paddar area, different discrimination plots have been discussed below.

According to Zhou *et al.* (2005), the higher-Al, lower-Cr spinels found in peridotites are produced in a MORB setting by low degrees of partial melting of the fertile upper mantle, whereas the higher-Cr, lower Al-Cr spinel are distinctive to a subduction zone tectonic setting and are produced by higher degrees of partial melting of a depleted mantle. The investigated chromite's $Cr\#$ (0.71–0.87) is similar to that of the layered igneous intrusions from Bushveld and Stillwater (Irvine 1967), higher than that of the mid-ocean ridge tholeiitic source magma (Allen *et al.* 1988), and lower than that of the boninites ($Cr\# = 0.80–0.90$; Roeder and Reynolds 1991). On plotting the calculated alumina percentage of parent melt and chromite in binary Al_2O_3 in melt *vs.* Al_2O_3 spinel plot (Kamenetsky *et al.* 2001; Rollinson 2008), the analysed chromites plot very close to the evolutionary trend of an arc system (figure 9b). They exhibit affinity towards the komatiites with higher Cr number, while lower Mg number in the $Cr\#$ *vs.* $Mg\#$ plot (figure 9c). Dick and Bullen (1984) noted

that spinels with high Cr# have parent magmas of the boninitic type that are richer in magnesium. According to Kostopoulos (1991), spinels with $\text{Cr\#} > 0.70$ are thought to be the product of partial melting at high temperatures that produce dunites free of pyroxene. Similar considerations have been made by other authors (Arai 1992; Zhou *et al.* 1994). The higher Cr# (0.71–0.87) from investigated chromite indicates that parent magma was Mg enriched and generated at higher temperatures.

On plotting the chromite composition in TiO_2 vs. Al_2O_3 tectonic discrimination diagram (Kamenetsky *et al.* 2001), the studied chromite occupies the high-Ti arc to supra-subduction field with wide TiO_2 and less Al_2O_3 variation (figure 9d). Dick and Bullen (1984) claimed that spinels with a greater Cr# (>60%) are typical of volcanic arcs, stratiform complexes, and oceanic plateau basalts, whereas spinels with a lower Cr# (60%) are indicative of oceanic crust. Therefore the arc-related tectonic environment is suggested for the studied ultramafic rocks. On plotting the chromite in Cr# against Mg# (figure 9e), studied chromites plot in and near the supra-subduction peridotites field showing the geochemical characteristics more similar to the spinel-chromites from Zildat peridotites. According to Singh's (2009) research, the Manipur Ophiolite Complex's peridotites contain chromian spinels (Cr-spinels) that have low Cr# (10.75–26.37) values and high Al# (72.71–88.36) and Mg# (70.00–73.43) values. They exhibit affinities with MORB at low partial melt rates, which are tholeiitic melt-derived abyssal and alpine-type peridotites. In ternary Cr–Al– $\text{Fe}^{3+} + 2\text{Ti}$, chromite from Paddar area occupy the Alpine peridotite field towards the Cr-rich end away from the Manipur Ophiolite Complex (figure 9f).

The geochemical characteristics of the chromite suggest a supra-subduction zone (SSZ) ophiolite geodynamic setting for the chromite origin (figure 10). Ultramafic magma was generated from the upper mantle and intruded into HHC unit along the deep-seated shear zone (Darlang Shear Zone). During the exhumation, deep seated ultramafic were brought near the surface while partial melting of HHC resulted in the migmatization and due to movement along the MCT and DSZ, hydrothermal fluid was generated, which interacted with the chromite resulting in chromite alteration.

7. Conclusion

The ultramafic rocks of the study area are hosted by the gneissic rocks of HHC, occurring in the form of laccolith, lenses, and bulbous bodies. They are mineralogically characterised by olivine, pyroxene (major phase), phlogopite, chromite, and Fe-oxide (minor phase). The presence of serpentine, talc, anthophyllite, and tremolite indicates the interaction with hydrothermal fluids. Chromite undergoes alteration along fracture and grain boundaries, which is also supported by chromite geochemistry. It is geochemically characterised by higher $\text{Cr}/\text{Cr} + \text{Al}$ and $\text{Fe}^{2+}/\text{Fe}^{2+} + \text{Mg}$, while $\text{Mg}/\text{Mg} + \text{Fe}^{2+}$ and $\text{Fe}^{3+}/\text{Cr} + \text{Al}$ ratios are lower. Calculated Al_2O_3 of the parent melt ranges between 8.11 and 11.67 wt%. The $\text{Ti} + \text{Cr} \leftrightarrow \text{Al}$, $\text{Cr} \leftrightarrow \text{Fe}$, $\text{Fe} \leftrightarrow \text{Mg}$, $\text{Fe} + \text{Mg} \leftrightarrow \text{Al}$ substitution mechanism operated during the crystallisation of chromite. It crystallised under high temperature, pressure conditions, and lower oxygen fugacity. The geochemistry of chromite suggests an arc to supra-subduction tectonic for the chromite genesis. Moreover, the proposed model is the first attempt to elucidate the crystallisation of chromite from ultramafic rock of HHC.

Acknowledgements

The permission to conduct fieldwork and sample collection in the Paddar sapphire mining region from M/s J and K Minerals Limited is gratefully acknowledged by the authors. For the EPMA analysis, we are grateful to Dr Dinesh Pandit and Prof. N V Chalapathi Rao of the Department of Geology, Banaras Hindu University. We are grateful for Shri. Shakeel Ahmed Wani's companionship and assistance throughout the fieldwork.

Author statement

Both authors have read, reviewed, and approved the paper. Both the authors contributed equally to the study.

References

- Abzalov M Z 1998 Chrome-spinels in gabbro-wehrilite intrusions of the Pechenga area, Kola Peninsula, Russia: Emphasis on alteration features; *Lithos* **43(3)** 109–134.
- Ahmed A H, Arai S, Abdel-Aziz Y M, Ikenne M and Rahimi A 2009 Platinum-group elements distribution and spinel

- composition in podiform chromitites and associated rocks from the upper mantle section of the Neoproterozoic Bou Azzer ophiolite, Anti-Atlas, Morocco; *J. Afr. Earth Sci.* **55**(1–2) 92–104.
- Akmaz R M, Uysal I and Saka S 2014 Compositional variations of chromite and solid inclusions in ophiolitic chromitites from the southeastern Turkey: Implications for chromitite genesis; *Ore Geol. Rev.* **58** 208–224.
- Allen G C, Jutson J A and Tempest P A 1988 Characterisation of nickel-chromium-iron spinel-type oxides; *J. Nucl. Mater.* **158** 96–107.
- Arai S 1992 Chemistry of chromian spinel in volcanic rocks as a potential guide to magma chemistry; *Mineral. Mag.* **56**(383) 173–184.
- Arai S 1997 Control of wall-rock composition on the formation of podiform chromitites as a result of magma/peridotite interaction; *Resour. Geol.* **47**(4) 177–187.
- Bannister V, Roeder P and Poustovetov A 1998 Chromite in the Paricutin lava flows (1943–1952); *J. Volcanol. Geotherm. Res.* **87**(1–4) 151–171.
- Barnes S J 2000 Chromite in komatiites, II. Modification during greenschist to mid-amphibolite facies metamorphism; *J. Petrol.* **41**(3) 387–409.
- Barnes S J and Hill R E T 1995 Poikilitic chromite in komatiitic cumulates; *Mineral. Petrol.* **54**(1) 85–92.
- Barnes S J and Roeder P L 2001 The range of spinel compositions in terrestrial mafic and ultramafic rocks; *J. Petrol.* **42**(12) 2279–2302.
- Bartoli O, Acosta-Vigil A, Cesare B, Remusat L, Gonzalez-Cano A, Wälle M and Langone A 2019 Geochemistry of Eocene-Early Oligocene low-temperature crustal melts from Greater Himalayan Sequence (Nepal): A nanogranitoid perspective; *Contrib. Mineral. Petrol.* **174** 1–18.
- Basu A R and MacGregor I D 1975 Chromite spinels from ultramafic xenoliths; *Geochim. Cosmochim. Acta* **39** 937–945.
- Basu A R and MacGregor I D 1976 Chromite spinels from ultramafic xenoliths; In: *Chromium: Its physicochemical behavior and petrologic significance*, Pergamon Press, pp. 937–945.
- Bhat I M, Ahmad T and Rao D S 2019 Alteration of primary Cr-spinel mineral composition from the Suru Valley ophiolitic peridotites, Ladakh Himalaya: Their low-temperature metamorphic implications; *J. Earth Syst. Sci.* **128** 1–14.
- Bird M L and Clark A L 1976 Microprobe study of olivine chromitites of the Goodnews Bay ultramafic complex, Alaska, and the occurrence of platinum; *J. Res. US Geol. Surv.* **4**(6) 717–725.
- Boudier F, Mainprice D, Nicolas A and Barou F 2021 Textural insights into the significance of ophiolitic chromitites, with special reference to Oman; *Tectonophysics.* **814** 228972.
- Burkhard D J 1993 Accessory chromium spinels: Their coexistence and alteration in serpentinites; *Geochim. Cosmochim. Acta* **57**(6) 1297–1306.
- Cameron E N 1975 Post cumulus and subsolidus equilibrium of chromite and coexisting silicates in the Eastern Bushveld Complex; *Geochim. Cosmochim. Acta* **39** 1021–1033.
- Carosi R, Montomoli C, Rubatto D and Visonà D 2010 Late Oligocene high-temperature shear zones in the core of the Higher Himalayan Crystallines (Lower Dolpo, western Nepal); *Tectonics* **29**(4) 1–20.
- Carosi R, Montomoli C, Iaccarino S and Visonà D 2019 Structural evolution, metamorphism and melting in the Greater Himalayan Sequence in central-western Nepal; *Geol. Soc. Spec. Publ.* **483**(1) 305–323.
- DeCelles P G, Gehrels G E, Quade J, LaReau B and Spurlin M 2000 Tectonic implications of U–Pb zircon ages of the Himalayan orogenic belt in Nepal; *Science* **288**(5465) 497–499.
- Deer W A, Howie R A and Zussman J 1992 An Introduction to the rock-forming minerals; 2nd edn., Longman Scientific and Technical, Hongkong, 696p.
- Dewey J F and Bird J M 1970 Mountain belts and the new global tectonics; *J. Geophys. Res.* **75**(14) 2625–2647.
- Dick H J and Bullen T 1984 Chromian spinel as a petrogenetic indicator in abyssal and alpine-type peridotites and spatially associated lavas; *Contrib. Mineral. Petrol.* **86**(1) 54–76.
- DiPietro J A and Pogue K R 2004 Tectonostratigraphic subdivisions of the Himalaya: A view from the west; *Tectonics* **23**(5).
- Evans B W and Frost B R 1976 Chrome-spinel in progressive metamorphism – a preliminary analysis; In: *Chromium: Its physicochemical behavior and petrologic significance*, Pergamon Press, pp. 959–972.
- Frank W, Grasmann B, Guntli P and Miller C 1995 Geological map of the Kishtwar-Chamba-Kulu region (NW Himalayas, India); *Jahrbuch der Geologischen Bundesanstalt* **138**(2) 299–308.
- Fuchs G 1975 Contributions to the geology of the north-western Himalayas; *Geolog. Bundesanst.* **32**.
- Gargiulo M F, Bjerg E A and Mogessie A 2013 Spinel group minerals in metamorphosed ultramafic rocks from Río de Las Tunas belt, Central Andes, Argentina; *Geol. Acta* **11**(2) 133–148.
- González Jiménez J M, Kerestedjian T, Proenza Fernández J A and Gervilla Linares F 2009 Metamorphism on chromite ores from the Dobromirski ultramafic massif, Rhodope Mountains (SE Bulgaria); *Geologica Acta* **7**(4) 413–429.
- González-Jiménez J M, Reich M, Camprubí A, Gervilla F, Griffin W L, Colás V and Centeno-García E 2015 Thermal metamorphism of mantle chromites and the stability of noble-metal nanoparticles; *Contrib. Mineral. Petrol.* **170**(2) 1–20.
- Guillot S, Hattori K H, de Sigoyer J, Nägler T and Auzende A L 2001 Evidence of hydration of the mantle wedge and its role in the exhumation of eclogites; *Earth Planet. Sci. Lett.* **193**(1–2) 115–127.
- Haggerty S E 1991 Oxide mineralogy of the upper mantle; In: *Oxide minerals: Petrologic and magnetic significance* (ed.) Lindsey D H, *Rev. Mineral. Geochem.* **25** 355–415.
- Herren E 1987 Zaskar Shear Zone: Northeast-southwest extension within the Higher Himalayas (Ladakh, India); *Geology* **15** 409–413.
- Hoffman M A and Walker D 1978 Textural and chemical variations of olivine and chrome spinel in the East Dover ultramafic bodies, south-central Vermont; *Geol. Soc. Am. Bull.* **89**(5) 699–710.
- Honegger K 1983 Structures and metamorphism in the Zaskar Crystalline (Ladakh-Kashmir, India); Unpublished PhD Thesis, ETH Zurich.
- Inger S and Harris N B W 1992 Tectonothermal evolution of the High Himalayan crystalline sequence, Langtang Valley, northern Nepal; *J. Metamorph. Geol.* **10**(3) 439–452.
- Irvine T N 1965 Chromian spinel as a petrogenetic indicator: Part 1. Theory; *Can. J. Earth Sci.* **2**(6) 648–672.

- Irvine T N 1967 Chromian spinel as a petrogenetic indicator: Part 2. Petrologic applications; *Can. J. Earth Sci.* **4**(1) 71–103.
- Irvine T N 1977 Origin of chromite layers in the Muskox intrusion and other intrusions: A new interpretation; *Geology* **5** 273–277.
- Ishii T 1992 Petrological studies of peridotites from diapiric serpentinite seamounds in the Izu–Ogasawara–Mariana forearc, Leg 125; In: Proceedings of the ocean drilling program, scientific results **125** 401–414.
- Ishwar-Kumar C, Rajesh V J, Windley B F, Razakamanana T, Itaya T, Babu E V S S K and Sajeev K 2016 Petrogenesis and tectonic setting of the Bondla mafic–ultramafic complex, western India: Inferences from chromian spinel chemistry; *J. Asian Earth Sci.* **130** 192–205.
- Jan M Q and Windley B F 1990 Chromian spinel-silicate chemistry in ultramafic rocks of the Jijal complex, north-west Pakistan; *J. Petrol.* **31**(3) 667–715.
- Jonnalagadda M K, Benoit M, Harshe S, Tilhac R, Duraiswami R A, Grégoire M and Karmalkar N R 2022 Geodynamic evolution of the Tethyan lithosphere as recorded in the Spontang Ophiolite, South Ladakh ophiolites (NW Himalaya, India); *Geosci. Front.* **13**(1) 101297.
- Kamenetsky V S, Crawford A J and Meffre S 2001 Factors controlling chemistry of magmatic spinel: An empirical study of associated olivine, Cr-spinel and melt inclusions from primitive rocks; *J. Petrol.* **42**(4) 655–671.
- Kang J, Chen L M, Yu S Y, Zheng W Q, Dai Z H, Zhou S H and Ai Q X 2022 Chromite geochemistry of the Jinchuan Ni–Cu sulfide-bearing ultramafic intrusion (NW China) and its petrogenetic implications; *Ore Geol. Rev.* **141** 104644.
- Kapsiotis A 2009 PGM and chromite mineralisation associated with the petrogenesis of the Vourinos and Pindos ophiolite complexes, northwestern Greece; Unpublished PhD thesis, University of Patras, Patras, Greece, 891p.
- Karipi S, Tsikouras B, Hatzipanagiotou K and Grammatikopoulos T A 2007 Petrogenetic significance of spinel-group minerals from the ultramafic rocks of the Iti and Kallidromon ophiolites (Central Greece); *Lithos* **99**(1–2) 136–149.
- Kimball K L 1990 Effects of hydrothermal alteration on the compositions of chromian spinels; *Contrib. Mineral. Petrol.* **105**(3) 337–346.
- Kostopoulos D K 1991 Melting of the shallow upper mantle: A new perspective; *J. Petrol.* **32**(4) 671–699.
- Kumar A, Lal N, Jain A K and Sorkhabi R B 1995 Late Cenozoic–Quaternary thermotectonic history of Higher Himalayan Crystallines (HHC) in Kishtwar–Padar–Zaskar region, NW Himalaya: Evidence from fission track ages; *J. Geol. Soc. India* **45** 375–391.
- Kundig R 1989 Domal structures and high-grade metamorphism in the Higher Himalayan Crystalline, Zaskar Region, north-west Himalaya, India; *J. Metamorph. Geol.* **7**(1) 43–55.
- Le Fort P 1996 Evolution of the Himalaya; In: *The tectonics of Asia* (eds) Yin A and Harrison T M, Cambridge University Press, New York, pp. 95–109.
- Liipo J, Vuollo J, Nykänen V and Piirainen T 1994 Chromite compositions as evidence for an Archaean ophiolite in the Kuhmo greenstone belt in Finland; *Bull. Geol. Soc. Finland* **66**(Part I) 3–18.
- Loferski P J and Lipin B R 1983 Exsolution in metamorphosed chromite from the Red Lodge district, Montana; *Am. Mineral.* **68**(7–8) 777–789.
- Maurel C and Maurel P 1982 Etude expérimentale de la solubilité du chrome dans les bains silicatés basiques et de sa distribution entre liquide et minéraux coexistants: Conditions d'existence du spinelle chromifère; *Bull. Mineral.* **105**(6) 640–647.
- Mills S J, Hatert F, Nickel E H and Ferraris G 2009 The standardisation of mineral group hierarchies: Application to recent nomenclature proposals; *Eur. J. Mineral.* **21**(5) 1073–1080.
- Moghadam H S, Khedr M Z, Arai S, Stern R J, Ghorbani G, Tamura A and Ottley C J 2015 Arc-related harzburgite–dunite–chromitite complexes in the mantle section of the Sabzevar ophiolite, Iran: A model for formation of podiform chromitites; *Gondwana Res.* **27**(2) 575–593.
- Nayak R and Maibam B 2020 Petrological study of spinel peridotites of Nidar ophiolite, Ladakh Himalaya, India; *J. Earth Syst. Sci.* **129**(1) 47.
- Noble S R and Searle M P 1995 Age of crustal melting and leucogranite formation from U–Pb zircon and monazite dating in the western Himalaya, Zaskar, India; *Geology* **23** 1135–1138.
- Onyeagocha A C 1974 Alteration of chromite from the Twin Sisters dunite, Washington; *Am. Mineral.: J. Earth Planet. Mater.* **59**(5–6) 608–612.
- Palache C, Berman H and Frondel C 1944 *The System of Mineralogy*; 7th edn., Wiley, New York, 834p.
- Parrish R R and Hodges V 1996 Isotopic constraints on the age and provenance of the Lesser and Greater Himalayan sequences, Nepalese Himalaya; *Geol. Soc. Am. Bull.* **108**(7) 904–911.
- Pognante U, Castelli D, Benna P, Genovese G, Oberli F, Meier M and Tonarini S 1990 The crystalline units of the High Himalayas in the Lahul–Zaskar region (northwest India): Metamorphic–tectonic history and geochronology of the collided and imbricated Indian plate; *Geol. Mag.* **127**(2) 101–116.
- Pogue K R, Hylland M D, Yeats R S, Khattak W U and Hussain A 1999 Stratigraphic and structural framework of Himalayan foothills, northern Pakistan; *Geol. Soc. Am. Spec. Papers*, pp. 257–274.
- Reddy S M, Searle M P and Massey J A 1993 Structural evolution of the High Himalayan gneiss sequence, Langtang valley, Nepal; *Geol. Soc. London, Spec. Publ.* **74**(1) 375–389.
- Roeder P L and Reynolds I 1991 Crystallisation of chromite and chromium solubility in basaltic melts; *J. Petrol.* **32**(5) 909–934.
- Rollinson H 2005 Chromite in the mantle section of the Oman ophiolite: A new genetic model; *Island Arc* **14**(4) 542–550.
- Rollinson H 2008 The geochemistry of mantle chromitites from the northern part of the Oman ophiolite: Inferred parental melt compositions; *Contrib. Mineral. Petrol.* **156**(3) 273–288.
- Rollinson H, Appel P W and Frei R 2002 A metamorphosed, early Archaean chromitite from west Greenland: Implications for the genesis of Archaean anorthositic chromitites; *J. Petrol.* **43**(11) 2143–2170.
- Saleh G M 2006 The chromite deposits associated with ophiolite complexes, southeastern Desert, Egypt: Petrological and geochemical characteristics and mineralisation; *Chin. J. Geochem.* **25**(4) 307–317.
- Saxena M N 1971 The crystalline axis of the Himalaya: The Indian shield and continental drift; *Tectonophysics.* **12**(6) 433–447.

- Scowen P A H, Roeder P L and Helz R T 1991 Reequilibration of chromite within Kilauea Iki lava lake, Hawaii; *Contrib. Miner. Petrol.* **107** 8–20.
- Searle M P, Stephenson B, Walker J and Walker C 2007 Restoration of the Western Himalaya: Implications for metamorphic protoliths, thrust and normal faulting, and channel flow models; *Episodes* **30(4)** 242.
- Singh R 2007 Geology of Kishtwar region, Jammu and Kashmir Himalaya, India with special emphasis on the Salkhalas, central crystallines; their relationship and implication on main central thrust; *J. Geol. Soc. India* **69(4)** 699.
- Singh A K 2009 High-Al chromian spinel in peridotites of Manipur Ophiolite Complex, Indo-Myanmar Orogenic Belt: Implication for petrogenesis and geotectonic setting; *Curr. Sci.* **96(7)** 973–978.
- Singh K 2010 Tectonic evolution of Kishtwar window with respect to the Main Central Thrust, northwest Himalaya, India; *J. Asian Earth Sci.* **39(3)** 125–135.
- Sorkhabi R B, Jain A K, Itaya T, Fukui S, Lal N and Kumar A 1997 Cooling age record of domal uplift in the core of the Higher Himalayan Crystallines (HHC), southwest Zaskar, India; *Proc. Indian Acad. Sci. (Earth Planet. Sci.)* **106(3)** 169–179.
- Srivastava P K and Singh P 2022 Geochemistry of tourmaline of elbaite-dravite series from sapphire bearing pegmatites, proterozoic higher Himalayan Crystalline Complex Jammu and Kashmir, India: Implication for evolution of pegmatite melt; *Lithos* **408** 106546.
- Staubli A R 1988 Metamorphism and deformation in the area of the main central displacement (MCT) (Kishtwar Park, central Himalaya). Geological Society of America Bulletin, Fenster, NW-Himalaya; PhD thesis no. 8573, ETH Zurich.
- Staubli A 1989 Polyphase metamorphism and the development of the Main Central Thrust; *J. Metamorph. Geol.* **7(1)** 73–93.
- Stephenson B J, Waters D J and Searle M P 2000 Inverted metamorphism and the Main Central Thrust: Field relations and thermobarometric constraints from the Kishtwar Window, NW Indian Himalaya; *J. Metamorph. Geol.* **18(5)** 571–590.
- Stephenson B J, Searle M P, Waters D J and Rex D C 2001 Structure of the Main Central Thrust zone and extrusion of the High Himalayan deep crustal wedge, Kishtwar–Zaskar Himalaya; *J. Geol. Soc.* **158(4)** 637–652.
- Stevens R E 1944 Composition of some chromites of the western hemisphere; *Am. Mineral.* **29(1–2)** 1–34.
- Takahashi E 1987 Primary magma compositions and Mg/Fe ratios of their mantle residues along Mid-Atlantic Ridge 29°N to 73°N; Technical Rept. ISEL, Ser. A **9** 1–14.
- Tewari A P 1981 Exotic thrust mass of the Padar area in Kashmir; *Tectonophysics*. **73** 285–294.
- Thakur V C 1980 Tectonics of the Central Crystallines of western Himalaya; *Tectonophysics*. **62(1–2)** 141–154.
- Thakur V C 1987 Plate tectonic interpretation of the western Himalaya; *Tectonophysics*. **134(1–3)** 91–102.
- Thöni M, Miller C, Hager C, Grasemann B and Horschneegg M 2012 New geochronological constraints on the thermal and exhumation history of the Lesser and Higher Himalayan Crystalline Units in the Kullu-Kinnaur area of Himachal Pradesh (India); *J. Asian Earth Sci.* **52** 98–116.
- Thy P 1983 Spinel minerals in transitional and alkali basaltic glasses from Iceland; *Contrib. Mineral. Petrol.* **83(1–2)** 141–149.
- Ulmer G C 1974 Alteration of chromite during serpentinisation in the Pennsylvania–Maryland District; *Am. Mineral.* **59(11–12)** 1236–1241.
- Waterton P, Pearson D G, Mertzman S A, Mertzman K R and Kjarsgaard B A 2020 A fractional crystallisation link between komatiites, basalts, and dunites of the Palaeoproterozoic Winnipegosis Komatiite Belt, Manitoba, Canada; *J. Petrol.* **61(5)** 052.
- Webb A A G, Schmitt A K, He D and Weigand E L 2011 Structural and geochronological evidence for the leading edge of the Greater Himalayan Crystalline complex in the central Nepal Himalay; *Earth Planet. Sci. Lett.* **304(3–4)** 483–495.
- Yang C, Liu S A, Zhang L, Wang Z Z, Liu P P and Li S G 2021 Zinc isotope fractionation between Cr-spinel and olivine and its implications for chromite crystallisation during magma differentiation; *Geochim. Cosmochim. Acta* **313** 277–294.
- Zaccarini F, Garuti G, Proenza J A, Campos L, Thalhammer O A, Aiglsperger T and Lewis J F 2011 Chromite and platinum group elements mineralisation in the Santa Elena Ultramafic Nappe (Costa Rica): Geodynamic implications; *Geol. Acta* **9(3–4)** 407–423.
- Zakrzewski M A 1989 Chromian spinels from Kusa, Bergslagen, Sweden; *Am. Mineral.* **74(3–4)** 448–455.
- Zhou M F and Kerrich R 1992 Morphology and composition of chromite in komatiites from the Belingwe greenstone belt, Zimbabwe; *Can. Mineral.* **30(2)** 303–317.
- Zhou M F and Robinson P T 1994 High-Cr and high-Al podiform chromitites, Western China: Relationship to partial melting and melt/rock reaction in the upper mantle; *Int. Geol. Rev.* **36(7)** 678–686.
- Zhou M F, Robinson P T and Bai W J 1994 Formation of podiform chromitites by melt/rock interaction in the upper mantle; *Miner. Depos.* **29** 98–101.
- Zhou M F, Robinson P T, Malpas J and Li Z 1996 Podiform chromitites in the Luobusa ophiolite (southern Tibet): Implications for melt-rock interaction and chromite segregation in the upper mantle; *J. Petrol.* **37(1)** 3–21.
- Zhou M F, Sun M, Keays R R and Kerrich R W 1998 Controls on platinum-group elemental distributions of podiform chromitites: A case study of high-Cr and high-Al chromitites from Chinese orogenic belts; *Geochim. Cosmochim. Acta* **62(4)** 677–688.
- Zhou M F, Robinson P T, Malpas J, Edwards S J and Qi L 2005 REE and PGE geochemical constraints on the formation of dunites in the Luobusa ophiolite, southern Tibet; *J. Petrol.* **46(3)** 615–639.
- Zhou M F, Robinson P T, Su B X, Gao J F, Li J W, Yang J S and Malpas J 2014 Compositions of chromite, associated minerals, and parental magmas of podiform chromite deposits: The role of slab contamination of asthenospheric melts in suprasubduction zone environments; *Gondwana Res.* **26(1)** 262–283.